A primer on the use of the nano3DX high-resolution X-ray microscope

Yoshihiro Takeda* and Kensaku Hamada*

1. Introduction

The nano3DX is an X-ray microscope with submicron spatial resolution, employing a quasi-parallel beam, near-detector system comprised of a unique high-intensity X-ray source and a high-resolution X-ray detector[1]. By selecting the X-ray energy to that is most appropriate for the sample, the instrument is capable of observing the microstructure of various samples such as pharmaceuticals, biological tissues, organic composite materials, and electronic materials, in either 2D (X-ray photography) or 3D (computed tomography) modalities, even where the differences in the density of sample components are not significant[2].

The nano3DX can be used for a number of different applications, and provides various structural information. For example, the observation of a pharmaceutical tablet allows us to characterize its structural features including flacking, cracking and density distribution inside the tablet as well as the features of the coat layer including its thickness and cracking/flacking in it. With organic composite materials, one would observe the orientation of filler and fibers, peeling of the filler and/or fiber off the base material, and the distribution/orientation of voids. In observation of biological tissues, one might want to visualize the structure of small tissues or even measure their length.

While the nano3DX will provide good results using the default measurement condition, fine tuning the measurement parameters often improves the result for a specific application. This article is intended to provide the readers with a basic knowledge of X-ray absorption, X-ray projected images, and computed tomography that can be utilized to design the optimum measurement for their purposes. Actual measurement examples using the nano3DX will be given to elucidate basic principles of X-ray microscopes and how one can choose measurement parameters for obtaining high-quality data.

2. Imaging using X-rays

Conventional X-ray photographs are X-ray projection images. X-rays which pass through the object reach the film, and the film records the features of the sample such as bones and lungs as a two-dimensional pattern of variations in density that corresponds to the intensity of the transmitted X-rays. This principle relies on the fact that the transmission of X-rays differs depending on the material and size of the sample.

In most imaging applications, the transmission of X-rays can be estimated adequately enough by taking only the absorption into account. This is because refraction and reflection of X-rays are negligibly small.

X-rays are absorbed according to the Beer-Lambert law. The intensity I of an X-ray which passes through a material is found as follows[3].

$$I=I_0 e^{-\int \mu_m \rho dl} = I_0 e^{-\int \mu dl} \quad (1)$$

Here, I_0 is the intensity of the incident X-ray, μ_m is the mass absorption coefficient, ρ is the material density, and μ is the linear absorption coefficient. It is immediately apparent that X-ray absorption is greater with a longer X-ray path or a higher density of the material.

The value of μ depends on the element type and X-ray energy, and, in the range of a few keV to a few tens of keV used in X-ray microscopes, it is approximately as follows.

$$\mu \propto Z^3 E^{-3} \quad (2)$$

This tells that the linear absorption coefficient increases exponentially with increasing atomic number (Z) and decreasing the X-ray energy (E). Some examples are shown in Fig. 1[4]–[6]. Poly(methyl methacrylate), PMMA, known more commonly as acrylic resin, is comprised of C, O and H, and has a larger linear absorption coefficient than polypropylene, PP, which is comprised of C and H only. The linear absorption coefficient of Al, with an atomic number of 13, is about 100 times that of PP and PMMA, and Ti with atomic number 22 has a coefficient about 10 times that of Al, and about 1000 times those of organic materials.

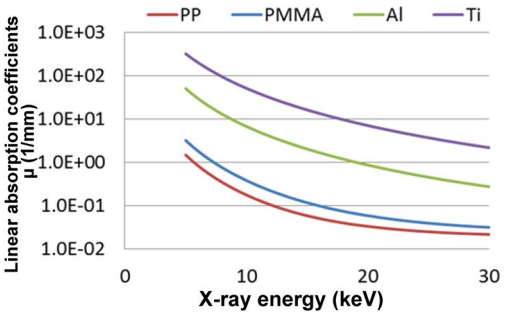

Fig. 1. X-ray energy and X-ray absorption coefficients.
PP: Polypropylene, PMMA: Poly (methyl methacrylate), Al: Aluminum, Ti: Titanium.

* X-ray Research Laboratory, Rigaku Corporation.

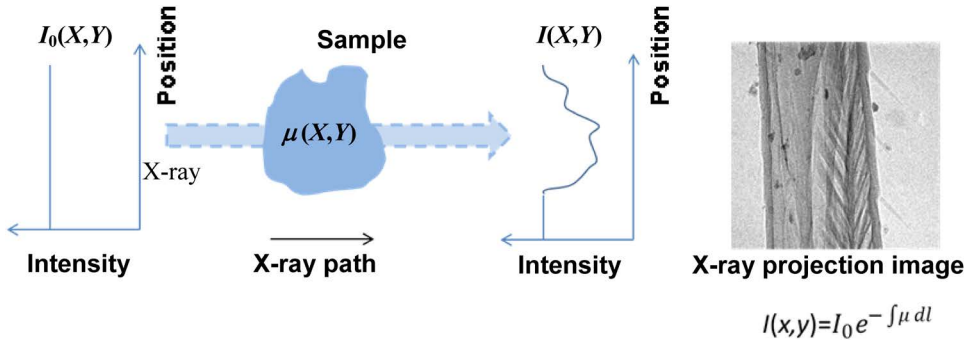

Fig. 2. X-ray transmission and X-ray projection image.

An X-ray projection image displays the differences in X-ray absorption between the chemical components inside the sample material as a black-to-white image-density distribution. The higher the atomic number of the material is, or the thicker the sample is, the more attenuated the X-rays that arrive at the X-ray detector are, and the darker the area appears in the projection image (Fig. 2).

The image contrast is greatly affected by the X-ray energy and the density of the sample. As Fig. 1 and Eq. (2) indicate, in materials comprised of light elements, such as carbon fiber reinforced plastic, absorption differences are small, especially with high-energy X-rays. While using low-energy X-rays improves the contrast of light-material images, it limits the maximum sample size.

To optimize the measurement conditions to obtain the best possible image quality, one should consider the parameters such as chemical components and the size of the sample, the available X-ray energy, and their effect on the resulting images. The concept applies to both simple projection imaging (2D X-ray imaging) and computed tomography (3D X-ray imaging), which will be explained in the following section.

3. Computed tomography

In an X-ray projection image, the structural information along a single optical path is integrated into a single point. This means the three-dimensional structural information is lost. On the other hand, computed tomography (CT) records the three-dimensional distribution of the X-ray absorption[7]–[9], allowing the user to retrieve the internal structure of the sample and to visualize the data in various formats including two-dimensional mapping on an arbitrary tomographic plane.

The following subsections describe the three steps comprising a CT procedure: CT measurement, CT reconstruction, and 3D display.

Step 1: CT measurement

X-ray projection images for the CT procedure are comprised of three-dimensional matrices of X-ray transmission intensities, $I(x, y, \theta)$, obtained by photographing the sample from multiple directions (Fig. 3). Here, θ is the sample rotation axis which is parallel with the y-axis, and x and y are the coordinates on the projection-image plane. While conventional CT systems that utilize image magnification by a divergent beam (cone beam) require a full 360° scan in θ, the nano3DX requires no more than a half-scan, or a θ scan from 0° through 180°. This is because the nano3DX, which utilizes a quasi-parallel beam, provides redundant data at θ and $\theta+\pi$.

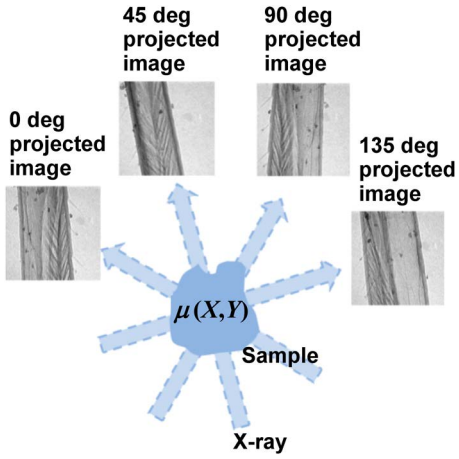

Fig. 3. CT measurement.
Photography of projection images of the sample from many directions.

Typically, projection images are acquired at 100−1000 different θ positions. The required number of projections varies depending on the desired spatial resolution and field of view[10]. The total time required for a CT measurement is, therefore, at least (the number of projections)×(exposure time per projection) and can reach several tens of minutes to several hours with a typical exposure time per projection of several seconds.

Step 2: CT reconstruction

CT reconstruction is the process of obtaining a tomographic image from the projected images $I(x, y, \theta)$ taken at different θ positions as described in Step 1. The linear absorption coefficient distribution $\mu(x, z)$ on the virtual tomographic plane is obtained from the projected images by carrying out a back-projection calculation (Fig. 4). By repeating this calculation over the whole

y range, it is possible to obtain the 3D distribution of the linear absorption coefficients $\mu(x, y, z)$. Applying a numerical filter to the projection images sometimes helps to obtain clearer CT data. The CT reconstruction involves a very large number of calculations, and, thus, requires a high-performance computer. CT reconstructed images are usually visualized as a negative image, where low absorption areas are shown in black.

Step 3: 3D display

A 3D image obtained through CT reconstruction is comprised of "slices," which are two-dimensional images parallel to the plane orthogonal to the sample rotation axis (x–z plane), stacked along the rotation axis (y). There are two methods to visualize the data: orthogonal 3 cross-section display multi-planar reconstruction (MPR), and volume rendering (VR) for three-dimensional display.

Figure 5 shows an example of MPR. (a), (b), and (c) are the tomographic images in the x–z plane, y–z plane, and x–y plane, respectively, each being perpendicular to the other two. The position along the axis perpendicular to the plane can be chosen arbitrarily.

Figure 6 shows an example of VR. This enables a bird's-eye display of a 3D image of the sample, and the image can also be easily enlarged or rotated. Furthermore, cross-sectional planes can be displayed, and the inside of the subject can be viewed.

For both MPR and VR, sophisticated rendering can be done using the system's various graphics functions such as color-coding of structures in accordance with the linear absorption coefficient.

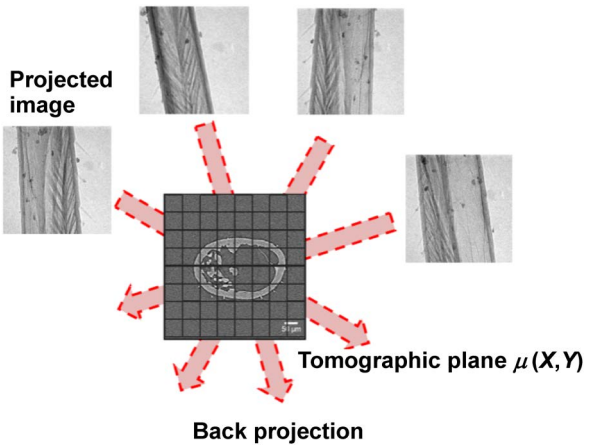

Fig. 4. CT reconstruction.
Back-projection is performed onto the projection images from multiple directions.

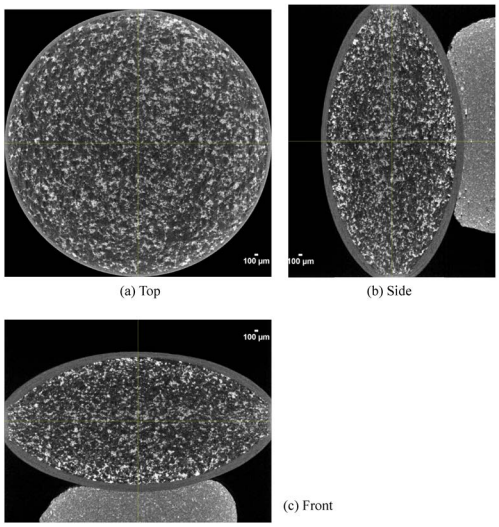

Fig. 5. Orthogonal 3 cross-section (MPR) display of a tablet.

4. For the best CT images —Setting the CT measurement parameters—

In CT measurements, there are multiple parameters that affect the final image quality. Although the nano3DX has carefully-chosen default values for many of these, the user often needs to adjust some parameters to optimize the system for specific purposes, such as determining the approximate shape of the sample as quickly as possible, or obtaining a CT dataset with a sufficiently high quality for a specific type of analysis. This section describes some tips and considerations for choosing suitable CT measurement parameters under given conditions.

Step 1: Choice of X-ray radiation (X-ray target) based on sample transmission thickness and contrast

With the nano3DX, the user can choose Mo, Cu or Cr as the X-ray target. The energies of the major characteristic X-rays from these materials are 17.5 keV, 8.0 keV and 5.4 keV, respectively. Figure 7 shows the results of a foam resin sample using the different X-ray targets. The resulting images indicate that the image contrast of the foam resin improves from Mo, Cu to Cr. Generally, good contrast can be obtained by choosing an appropriate X-ray target to suit the sample material, size and the density differences between the components. While the foam resin, a low-density material, gave good images with Cr radiation, samples with higher-density components or larger samples might be better

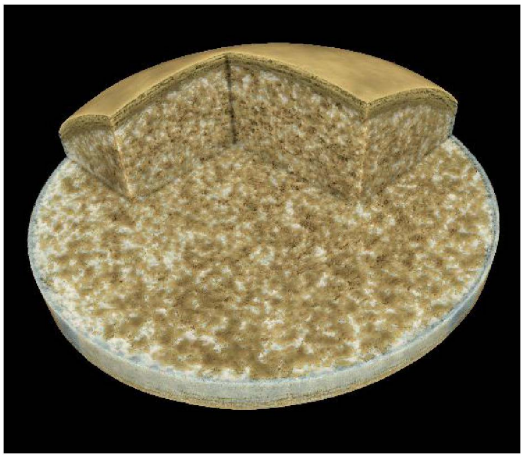

Fig. 6. Volume rendering (VR) display of of the tablet in Fig. 5.

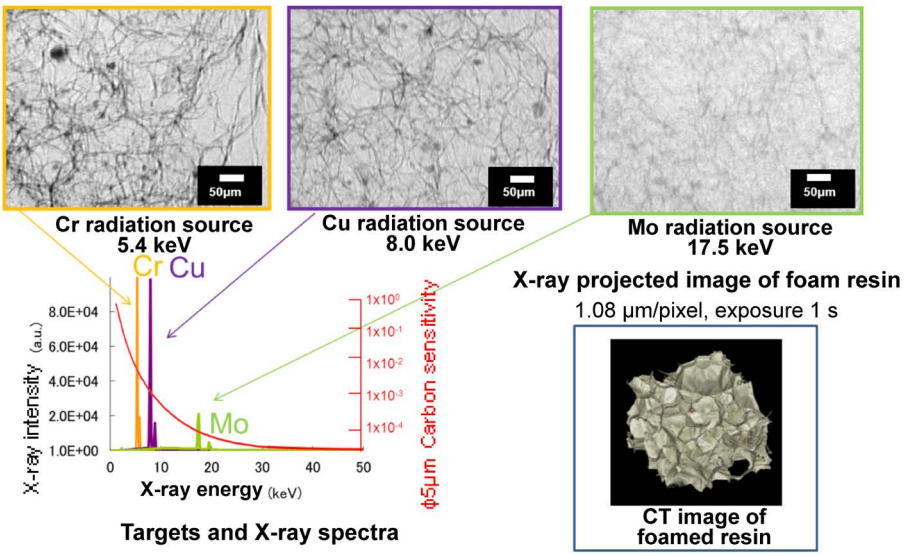

↑ High-sensitivity, small sample
Cr: Polymer blends, biological samples, etc. Organic material transmission thickness to 1 mm
Cu: Light element composite materials (carbon fiber reinforced plastic), pharmaceutical granulated particles, etc. Organic material transmission thickness to a few mm
Mo: Light metals, ceramics, materials containing fillers, tablets. Organic material transmission thickness to 20 mm
↓ High transmittance

Fig. 7. X-ray imaging and differences in X-ray spectra depending on the target.

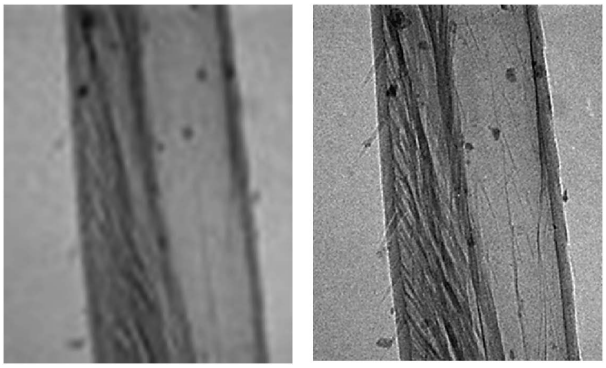

Low-resolution image
9.6 μm/pixel (4×4 binning)

High-resolution image
2.4 μm/pixel

Fig. 8. Comparison of projected images with different resolutions.

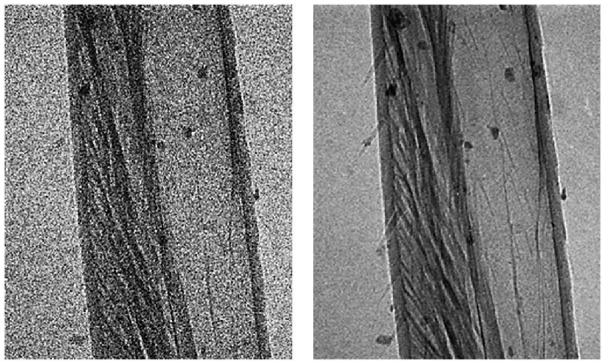

Low S/N ratio image
S/N ratio=4
Exposure time: short

High S/N ratio image
S/N ratio=15
Exposure time: long

Fig. 9. Comparison of projection images with different exposure time.

observed using the Mo target. The Cu target is often suitable for carbon fiber reinforced polymer, CFRP, which are comprised of epoxy resin and carbon fibers. However, the choice of target material also depends on the sample size. In addition, measurements of organic samples with small density differences are often easier to perform with Cr radiation than with the other targets because the differences in linear absorption coefficient between different light-weight components is larger with Cr radiation. Using Cr radiation, however, requires the sample thickness to be 1 mm or less because of the X-ray transmission would be very small otherwise.

Step 2: Selection of X-ray detector lens based on required field of view and spatial resolution

With the nano3DX, both the field of view and the pixel size are determined by the lens of the X-ray detector. Therefore, the lens of the X-ray detector should be selected to suit the required field of view and resolution.

The pixel size can be modified without changing the lens by changing the "binning" setting. If 2×2 binning is selected, the pixel size is doubled, the exposure time is reduced by 75%, and the size of CT reconstruction data, which would be about 25 GB with no binning, is also reduced to about 3.3 GB. Therefore, CT measurement can be done more efficiently by selecting a resolution that best suits the purpose. For example, Fig. 8 shows an example of differences in spatial resolution using the same sample.

Step 3: Determination of exposure time

A longer exposure time gives the projected images a higher-S/N ratio while a shorter exposure time makes it more difficult to observe fine structures and to visualize the small differences in density (Fig. 9). As already mentioned in Step 2, the binning setting has a large influence on the exposure time. Doubling the pixel size can reduce the exposure time to 1/4 at the expense of resolution.

Step 4: Determination of the number of projections

After the X-ray target, field of view, resolution and exposure time have been determined, the next step is determining the number of projections for CT measurement. The spatial resolution and the S/N ratio are improved by obtaining more projections for CT reconstruction. As explained in "**3. Computer tomography, Step 2: CT reconstruction**," the required number of projections is found through calculation based on the resolution and field-of-view width. In practical applications, however, it is often sufficient to use a number of projections smaller than that. Although it depends on the shape of the sample, Eq. (3) can be used as a guideline in choosing the necessary number of projections. In many cases, this gives 300–1000 projections in a 180° range.

$$\text{Number of projections} \propto \frac{\text{Sample size}}{\text{Resolution}} \tag{3}$$

Figure 10 demonstrates the effect of the number of projections on the quality of a CT reconstructed image.

While a simple observation of the approximate shape of a sample can be done with 100 projections or less, more detailed data processing such as 3D analysis require more projections.

4.1. Actual example using a sugar-coated tablet

The effect of the resolution on the S/N ratio (exposure time) is demonstrated using a sugar-coated tablet as the sample. The Mo radiation was used for the experiment. Figure 12 shows a 2×2 mm internal section of the tablet shown in the projected image in Fig. 11.

4.1.1. Differences due to resolution

When the CT measurement was performed at 2.16 μm/pixel, each particle was imaged clearly. Voids (the blackest areas) and line-shaped cracks were also clearly shown. When the CT measurement was done at 8.64 μm/pixel, the image became less clear, however, particles could still be discriminated. In the CT at 13 μm/pixel, where voids could also be clearly confirmed at 2.16 μm/pixel, it was possible to discriminate high density particles (white), but it was almost impossible to confirm voids and cracks.

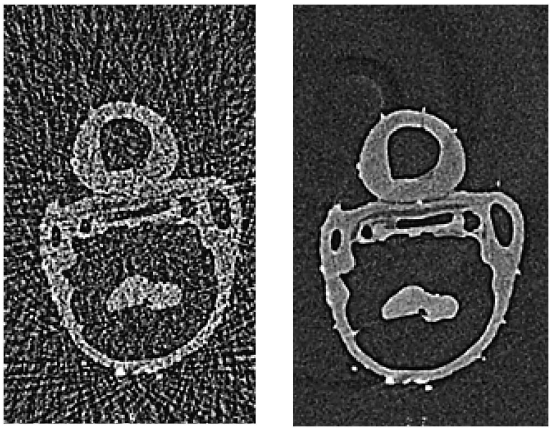

Number of projections: small
36 projections/180°

Number of projections: large
360 projections/180°

Fig. 10. Differences in CT reconstructed images based on the number of projections.

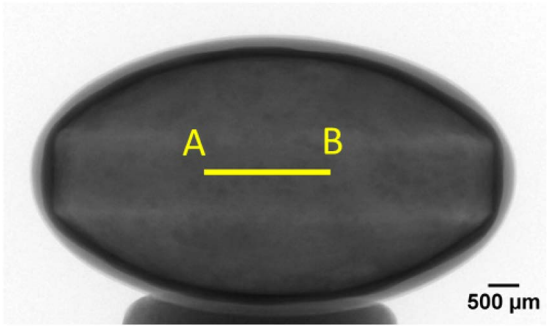

Fig. 11. Projected image of sugar-coated tablet.

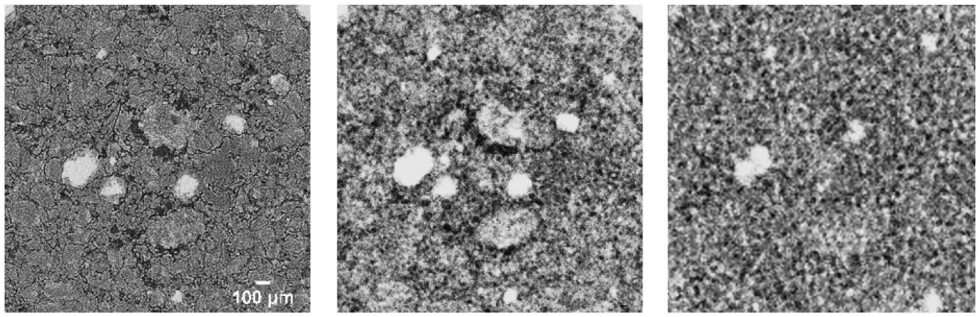

2.16 μm/pixel
Data capacity: 3 GB

8.64 μm/pixel
Data capacity: 0.3 GB

13 μm/pixel
Data capacity: 0.1 GB

Fig. 12. A–B tomographic plane measured while varying resolution for a CT reconstructed image.

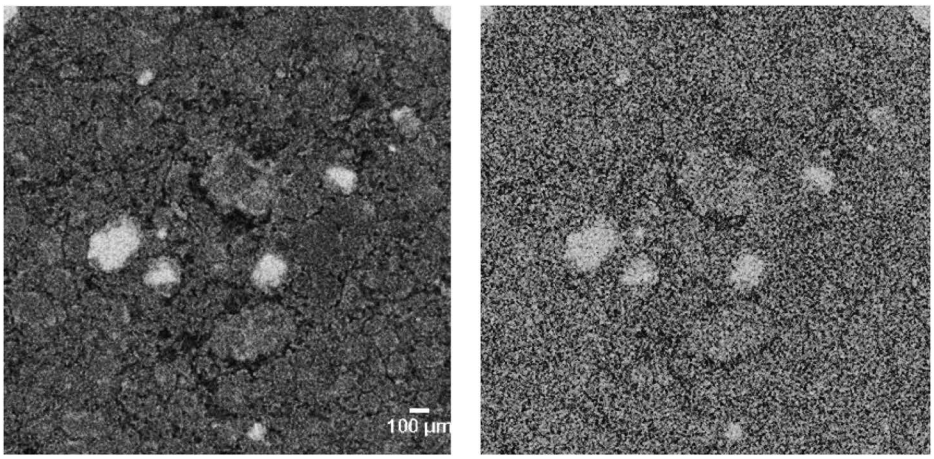

Exposure 8 s, 4.32 μm/pixel, 720 projections Exposure 1 s, 4.32 μm/pixel, 720 projections

Fig. 13. A−B tomographic plane measured while varying exposure time, CT reconstructed image.

4.1.2. Differences due to exposure time

In Fig. 13 we see the results of a measurement with an exposure time of 8 seconds. Each particle was clearly distinguished, and voids and cracks could also be clearly confirmed. In a CT measurement with an exposure time of 1 second, it was possible to confirm high-density particles and voids with sizes of a few 10 μm, but noise increased, and clarity of microstructure was lost.

5. Conclusion

This paper has explained a number of facts about X-ray imaging, i.e. that differences in linear absorption within a sample are converted into an image; and that X-ray absorption coefficients depend on the type, density and size of a material, as well as on the X-ray energy. The principles of CT and the measurement parameters which affect the CT image were also explained. Using a tablet as an example, the paper also touched on effects on images due to differences in resolution and exposure time.

References

(1) *Rigaku Journal (Japanese version)*, **43** (2012), No. 2, 28−30.
(2) Y. Takeda and K. Hamada: *Rigaku Journal (English version)*, **30** (2014), No. 1, 17−22 .
(3) H. P. Klug and L. E. Alexander: *X-ray Diffraction Procedures*, John Wiley & Sons. Inc. (1974).
(4) S. Sasaki: *KEK Report*, No. 88-14, National Laboratory for High Energy Physics, Tsukuba, (1989).
(5) S. Sasaki: *KEK Report*, No. 90-16, National Laboratory for High Energy Physics,Tsukuba, (1990).
(6) B. L. Henke, E. M. Gullikson and J. C. Davis: *Atomic Data and Nuclear Data Tables*, **54** (1993), 181−342.
(7) G. N. Hounsfield: *British J. Rad*, **46** (1973), 1016.
(8) R. Szeliski: *Computer Vision: Algorithms and Application*, Springer, UK, (2011).
(9) L. A. Feldkamp, L. C. Davis and J. W. Kress: *J. Opt. Soc. Am.*, **A1** (1984), 612−619.
(10) H. Toda, M. Kobayashi, Y. Suzuki, A. Takeuchi and K. Uesugi: *Microscope* (in Japanese), **44** (2009), No. 3, 199−205.